Integrated analyses of density, P-wave velocity, lithogeochemistry, and mineralogy to investigate effects of hydrothermal alteration and metamorphism on seismic reflectivity: a summary of results from the Lalor volcanogenic massive-sulfide deposit, Snow Lake, Manitoba†

E.M. Schetselaar[1]*, G. Bellefleur[1], and P. Hunt[1]

Schetselaar, E., Bellefleur, G., and Hunt, P., 2022. Integrated analyses of density, P-wave velocity, lithogeochemistry, and mineralogy to investigate effects of hydrothermal alteration and metamorphism on seismic reflectivity: a summary of results from the Lalor volcanogenic massive-sulfide deposit, Snow Lake, Manitoba; in *Targeted Geoscience Initiative 5: volcanic- and sediment-hosted massive-sulfide deposit genesis and exploration methods, (ed.) J.M. Peter and M.G. Gadd; Geological Survey of Canada, Bulletin 617, p. 329–344. https://doi.org/10.4095/327999*

Abstract: We present herein a summary of integrated data analyses aimed at investigating the effects of hydrothermal alteration on seismic reflectivity in the footwall of the Lalor volcanogenic massive-sulfide (VMS) deposit, Manitoba. Multivariate analyses of seismic rock properties, lithofacies, and hydrothermal alteration indices show an increase in P-wave velocity for altered volcanic and volcaniclastic lithofacies with respect to their least-altered equivalents. Scanning electron microscopy–energy dispersive X-ray spectrometry analyses of drill-core samples suggest that this P-wave velocity increase is due to the high abundance of high P-wave velocity aluminous minerals, including cordierite, Fe-Mg amphibole, and garnet, which in volcanic rocks are characteristic of VMS-associated hydrothermal alteration metamorphosed in the amphibolite facies. A seismic synthetic profile computed from a simple amphibolite-facies mineral assemblage model, consisting of mafic-felsic host rock contacts, a sulfide ore lens, and a discordant hydrothermal conduit, show enhanced seismic reflections at conduit-host rock contacts in comparison to the equivalent greenschist facies mineral assemblage model. Collectively our results suggest that VMS footwall hydrothermal alteration zones metamorphosed under middle- to upper-amphibolite facies conditions have enhanced potential for seismic detection.

Résumé : Nous présentons ici un résumé des analyses de données intégrées visant l'étude des effets de l'altération hydrothermale sur la réflectivité sismique dans l'éponte inférieure du gisement de sulfures massifs volcanogènes (SMV) à minéralisation polymétallique de Lalor, au Manitoba. Les analyses multivariées des propriétés sismiques des roches, des lithofaciès et des indices d'altération hydrothermale montrent un accroissement de la vitesse de propagation des ondes P dans les lithofaciès volcaniques et volcanoclastiques altérés par rapport à leurs équivalents moins altérés. Les analyses d'échantillons de carottes de forage par microscopie électronique à balayage couplée à la spectrométrie X à dispersion d'énergie laissent croire que cet accroissement de la vitesse de propagation des ondes P est attribuable à la grande abondance de minéraux alumineux présentant de fortes vitesses de propagation des ondes P, y compris la cordiérite, les amphiboles ferromagnésiennes et le grenat, dont la présence dans les roches volcaniques est caractéristique de l'altération hydrothermale associée aux SMV suite à un métamorphisme dans les conditions du faciès des amphibolites. Un profil sismique synthétique calculé à partir d'un modèle simple aux associations de minéraux du faciès des amphibolites, constitué de contacts entre des roches hôtes mafiques et felsiques, d'une lentille de minerai sulfuré et d'un conduit hydrothermal discordant, affiche des réflexions sismiques accrues aux contacts entre le conduit et les roches hôtes, comparativement au modèle équivalent aux associations de minéraux du faciès des schistes verts. Pris ensemble, nos résultats laissent croire que le métamorphisme des zones d'altération hydrothermale dans l'éponte inférieure du gisement de SMV dans les conditions du faciès des amphibolites inférieur à intermédiaire a amélioré le potentiel de détection du gisement par des méthodes sismiques.

[1]Geological Survey of Canada, 601 Booth Street, Ottawa, Ontario K1A 0E8
*Corresponding author: E. Schetselaar (email: ernst.schetselaar@nrcan-rncan.gc.ca)
†This contribution is a summary of an article published previously in the open access journal *Minerals*: Schetselaar, E.M., Bellefleur, G., and Hunt, P., 2019. Elucidating the effects of hydrothermal alteration on seismic reflectivity in the footwall of the Lalor volcanogenic massive sulfide deposit, Snow Lake, Manitoba, Canada; Minerals, v. 9, no. 6, 384. https://doi.org/10.3390/min9060384

INTRODUCTION

The seismic-reflection method has, during the past three decades, shown promising results in the exploration for volcanogenic massive-sulfide (VMS) deposits (Salisbury et al., 1996, 2000; Snyder and Salisbury, 2007; Malehmir et al., 2012). This success is largely attributable to the presence of high-density sulfide minerals in VMS ore, including minerals of low P-wave velocity, such as chalcopyrite, pyrrhotite, sphalerite, and minerals of high P-wave velocity, such as pyrite. The sulfide-dominant compositions of these deposits generally result in high impedance contrasts at contacts with the silicate-dominant volcanogenic host rocks (Salisbury et al., 1996, 2000; Snyder and Salisbury, 2007). Hydrothermal alteration zones provide a much larger secondary target for exploration, increasing the likelihood of detecting VMS deposits at greater depths. Seismic detection of such zones is challenging, however, because the effect of hydrothermal alteration on seismic impedance contrast is generally secondary to the variations associated with sulfide mineralization and lithological variations in the host rocks. Integrated analyses of seismic rock properties, whole-rock geochemistry, and mineral abundance estimates from scanning electron microscopy–energy dispersive X-ray spectrometry (SEM-EDS) analyses of the Lalor VMS deposit, Manitoba, were conducted to

1. assess if the effects of hydrothermal alteration on seismic properties, including P-wave velocity (defined as the velocity of compressional seismic waves propagating through Earth materials) and density, can be distinguished from those controlled by primary factors (e.g. lithological composition and sulfide ore minerals);
2. assess if the effects of hydrothermal alteration on seismic impedance (product of P-wave velocity and density) lead to detectable reflections by applying seismic forward modelling to a simplified model of a VMS deposit; and
3. outline the hydrothermal alteration zone on the Lalor 3-D seismic cube.

This contribution summarizes the main outcomes of a previously published paper on this topic (Schetselaar et al., 2019). We refer the reader to this paper for an in-depth discussion of the methodology and interpretation of the integrated analyses of seismic rock property, geochemical, and mineralogical data.

GEOLOGICAL SETTING

The Lalor VMS deposit is a zinc-rich VMS deposit hosted in a 1.89 Ga juvenile arc assemblage of the Snow Lake Domain (Fig. 1). The Snow Lake arc assemblage comprises a 6 km thick section of three volcanic successions displaying a geodynamic evolution from a primitive arc (Anderson Sequence to the south) to a mature arc (Chisel Sequence) to an arc-rift (Snow Creek Sequence to the northeast) setting (Bailes and Galley, 1999). The 1.89 Ga volcanic sequences were intruded by 1.88 to 1.84 Ga successor-arc felsic and mafic plutons, deformed by isoclinal folds and thrusts, and subsequently interleaved with 1.86 to 1.84 Ga successor-arc sedimentary cover as a result of progressive deformation (Kraus and Williams, 1999; Stewart et al., 2018), during which peak upper almandine- to amphibolite-facies metamorphic conditions were reached at approximately 1.82 to 1.81 Ga (Bailes and Galley, 1999).

A large subconcordant hydrothermal alteration system developed in the footwall of the Zn-rich VMS deposit, closely associated in space and time to the magmatic evolution of the Richards subvolcanic intrusion (Fig. 1; Bailes et al., 2016). Disconformable alteration zones can be traced from this pluton upsection to the Chisel, Chisel North, and Lalor deposits (Bailes et al., 2016). The footwall hydrothermal alteration in the Lower Chisel subsequence evolved in two stages. The first produced a semiconformable zone of albitization, silicification, and epidotization 1 to 2 km below the deposit that is spatially associated with synvolcanic dykes and intrusions. The second, which is the subject of this study, produced subconcordant zones of intense hydrothermal alteration in the immediate footwall of the massive-sulfide deposits, marking their feeder conduits (Bailes et al., 2016).

The hydrothermally altered rocks were, after amphibolite facies metamorphism, transformed into schist and gneiss rich in large aluminosilicate porphyroblasts of garnet, staurolite, cordierite, and kyanite, as well as anthophyllite (Caté et al., 2014; Bailes et al., 2016). Alteration in close proximity to the sulfide ore zones at Lalor also includes pervasive zones of finely disseminated sulfides (pyrite, pyrrhotite, sphalerite, chalcopyrite, and galena) associated with rocks rich in carbonate minerals, tremolite, talc, and chlorite (Caté et al., 2014; Bailes et al., 2016). Four chemical associations can be distinguished in the zone of intense hydrothermal alteration in the footwall of the Lalor VMS deposit based on metamorphic mineral assemblages (Table 1). These mineral assemblages reflect lithogeochemical variations of different volcanic protoliths, as well as metasomatism during hydrothermal alteration and subsequent metamorphic crystallization (Caté et al., 2014).

INTEGRATED ANALYSES OF SEISMIC WIRELINE LOGS AND DRILL CORE

Wireline-logging data acquired in 10 drillholes were used in previous interpretations to show that massive-sulfide mineralization and felsic to mafic host rock contacts generate the dominant high-amplitude seismic reflections at Lalor (Bellefleur et al., 2015; Schetselaar et al., 2017).

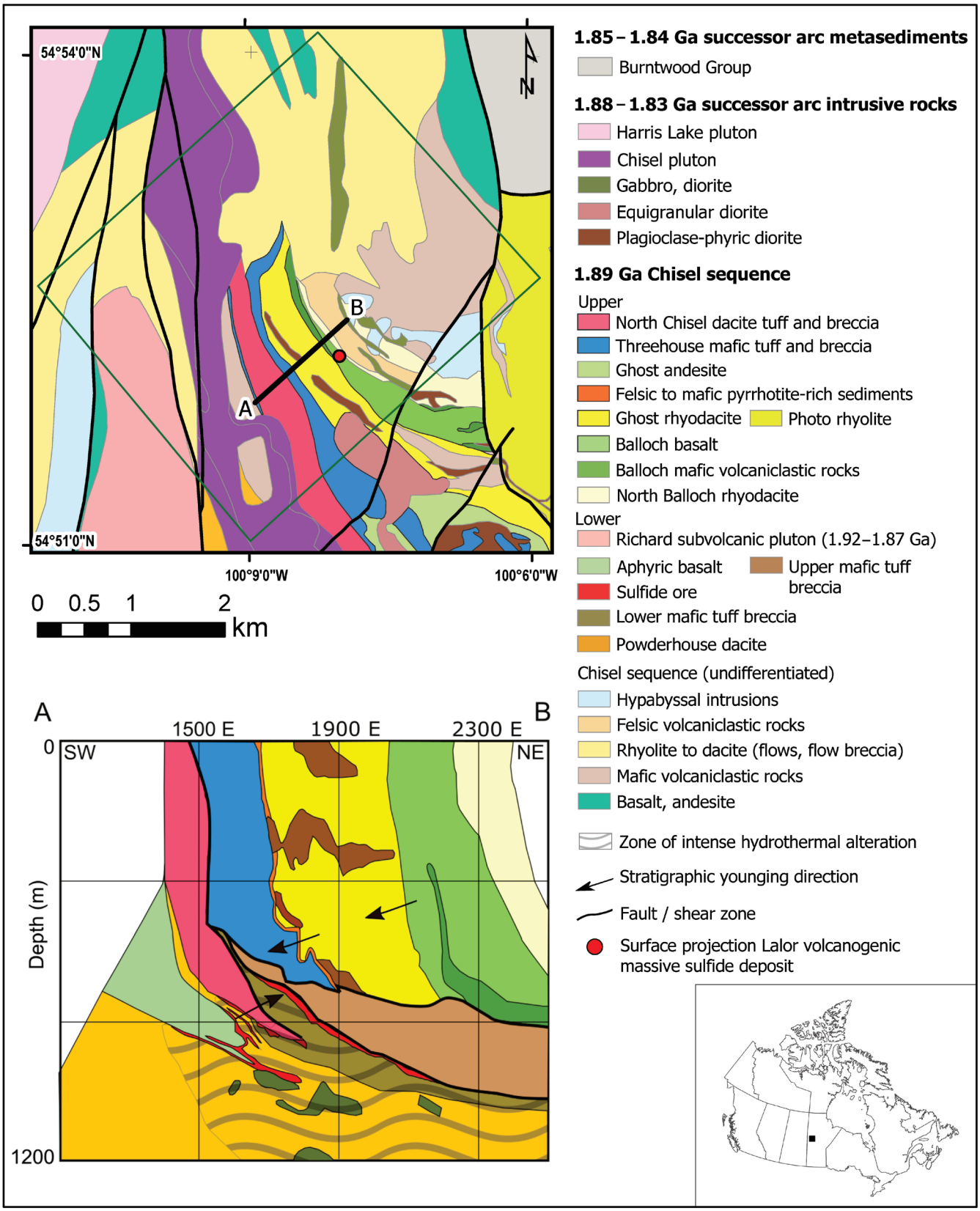

Figure 1. **a)** Geological map of the Chisel basin showing the outline of the 3-D seismic survey and **b)** the 5200 N section, a southwest-northeast–oriented cross section (A–B) of the Lalor volcanogenic massive-sulfide deposit (*after* Bailes and Galley, 2007).

Table 1. Chemical associations recognized in the footwall hydrothermal alteration zone of the Lalor VMS deposit.

Chemical association	Minerals
K	Sericite, pyrite, biotite, kyanite
K-Fe, Mg	Quartz, biotite, kyanite
Fe, Mg	Anthophyllite, cordierite, garnet, biotite, staurolite
Ca, Mg	Carbonate, chlorite±Ca-Mg amphiboles
Less intense alteration	Variable
After Caté et al., 2016.	

These wireline-log data were co-registered with drill-core geochemistry and their corresponding lithofacies using a threshold distance of 30 cm between sample locations along the drill path (Schetselaar et al., 2019).

In any assessment of the effects of hydrothermal alteration on seismic reflectivity, it is important to separate the effects of hydrothermal alteration (and subsequent metamorphism thereof) on acoustic impedance contrast from those caused by variations in protolith composition; therefore, our subdivision into lithofacies was based on immobile element ratios that allowed the drill-core samples to be grouped into lithofacies with felsic, intermediate, and intermediate to mafic protolith compositions (Caté, 2016). Each of these three lithofacies were further subdivided into least-altered and intensely altered groups, using the diagnostic metamorphic mineral assemblages of aluminosilicates listed in Table 1, yielding a total of six lithofacies classes.

The P-wave velocity (V_p) versus density (ρ) plot of the lithofacies categorization is shown in Figure 2. The overlay of ellipses shown in Figure 2b is determined from principal-component analysis of the P-wave velocity and density wireline-log data of each lithofacies. The ellipses represent the mean and scaled eigenvectors of the covariance matrix of the velocity-density distribution, so that the major and minor axes of the ellipses represent one standard deviation (i.e. 68%) of their distribution. The locations and dimensions of the ellipses of mafic and felsic lithofacies in V_p-ρ space show that protolith composition dominantly controls acoustic-impedance contrast for both least-altered and intensely altered lithofacies. This is consistent with high-amplitude reflections observed at the contacts between least-altered felsic and mafic lithofacies (Schetselaar et al., 2017). The second-order effects of hydrothermal alteration can be inferred by comparing the dimensions of the ellipses between least-altered and intensely altered lithofacies. Note that all the ellipses of the intensely altered lithofacies are significantly larger in comparison to their least-altered equivalents. In addition, the intensely altered lithofacies with intermediate to mafic protolith composition are oriented on a steeply sloping, but slightly negative trend.

Seismic-rock property variations were also analyzed with respect to the Ishikawa alteration index (AI) and chlorite-carbonate-pyrite index (CCPI), which are commonly used as proxies for the style and intensity of hydrothermal alteration in VMS ore systems (Large et al., 2001). Figure 3 shows V_p-ρ plots of the AI and CCPI computed from the drill-core geochemical analyses of intermediate to mafic protoliths. The AI and CCPI values increase with increasing P-wave velocities in these plots along a steep negatively correlated trend, which is consistent with the orientation of ellipses for altered lithofacies of intermediate to mafic composition (Fig. 2).

SCANNING ELECTRON MICROSCOPY–ENERGY DISPERSIVE X-RAY SPECTROMETRY ANALYSIS

To determine the minerals responsible for the negative low-density, high P-wave velocity trend, 11 polished thin sections of 4.5 × 2.5 cm from drill-core samples of the footwall of the Lalor deposit, cut normal to the foliation, were analyzed with SEM-EDS. Because no lineation was observed in the samples, it was assumed that the preferred mineral orientation, defining the foliation, interacted in an isotropic manner with these sections.

The thin sections were analyzed using a TESCAN MIRA$_3$ SEM equipped with an Oxford EDS (Oxford Instruments, 2020), which includes an X-MAX 80 silicon drift detector and AZtec Energy 3.3 microanalysis software (Oxford Instruments, undated). The specialized module 'Feature' of AZtec was used to classify minerals using the energy dispersive X-ray spectrometry (EDS) data. The individual mineral grains were identified using grey-level thresholding of backscattered electron images. Morphology and chemistry were then recorded for each grain and each spectrum was immediately quantified and classified according to a user-generated classification scheme. Many fields were recorded at high magnification and subsequently montaged together to image a large area. The adjoining mineral grains were then reconstructed across the whole area (Oxford Instruments, undated). With morphology and chemistry analyzed, the results enabled a full calculation of the bulk mineralogy of the entire section, including the percentage of unclassified features (Fig. 4, Table 2).

Given that the SEM-EDS analyses of the thin sections are limited to estimating mineral fractions, modelling seismic rock properties is bounded by two limiting assumptions: the seismic rock properties are completely defined by the constituting mineral phases (the effects of porosity, including microcracks, are negligible); and there is no preferential orientation of the mineral phases (e.g. the fabric of the rocks is homogeneous and quasi-isotropic). Under

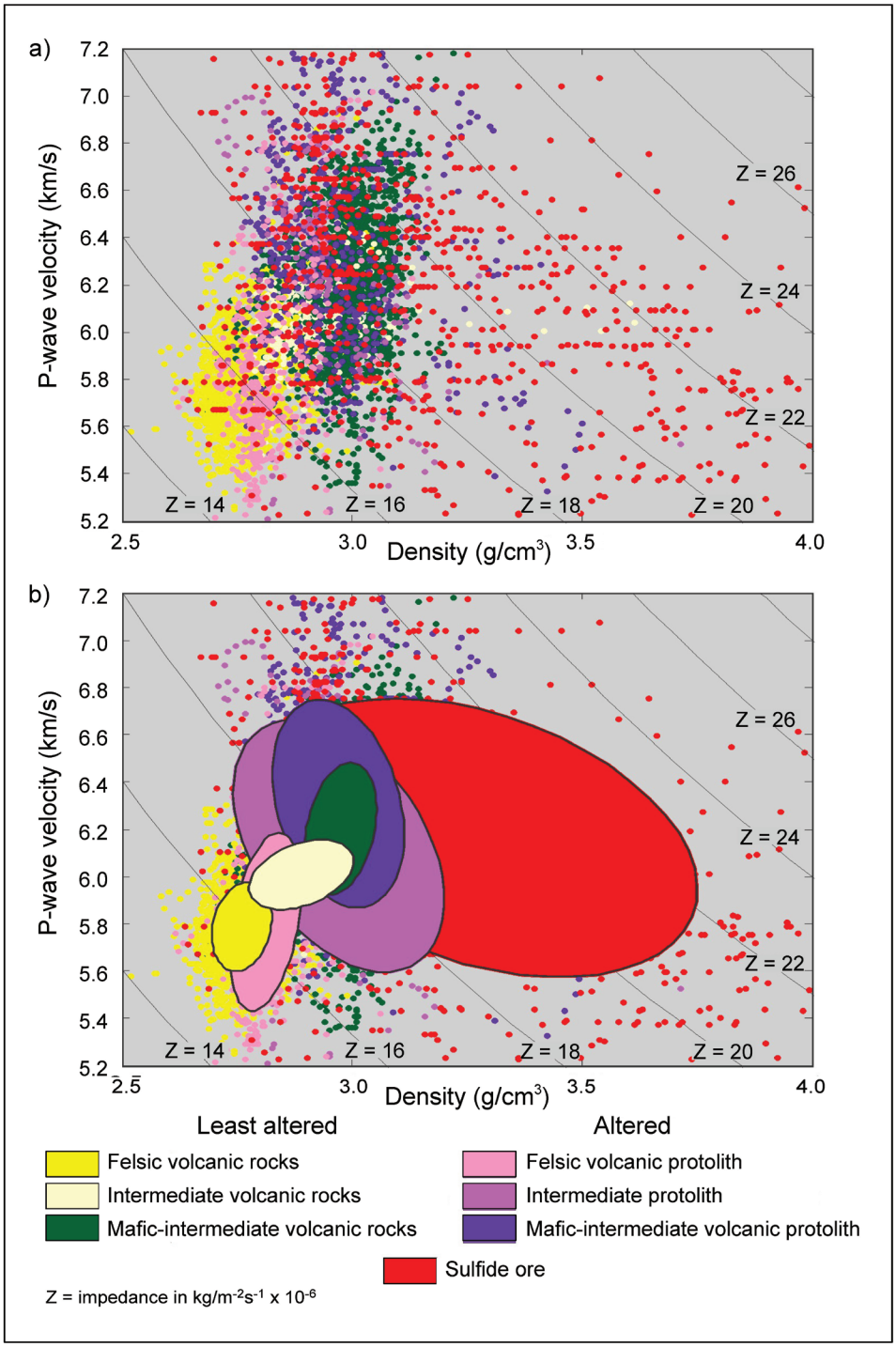

Figure 2. P-wave velocity (V_p) and density (ρ) wireline-log data of the main lithofacies units intersected in 10 drillholes. The undifferentiated ore lithofacies unit, including disseminated, vein-type, semi-massive, and massive-sulfide mineralization, was based on drill-log interval descriptions from HudBay Minerals (Schetselaar et al., 2017). The other lithofacies units are based on the Zr-Ti immobile element ratio from drill-core geochemistry and drill-log interval descriptions from HudBay Minerals (Schetselaar et al., 2017). Mafic to intermediate lithofacies was defined by Zr-Ti < 0.017, intermediate lithofacies by 0.017 ≤ Zr-Ti < 0.030, and felsic lithofacies by Zr-Ti ≥ 0.030: **a)** V_p-ρ plot of wireline-log measurements of lithofacies units; **b)** ellipses defined by principal component analysis of V_p and ρ for each lithofacies unit, with the minor and major axes representing one standard deviation from the mean, superimposed on the V_p-ρ plot presented in a). Lines of constant acoustic impedance (Z) are also shown.

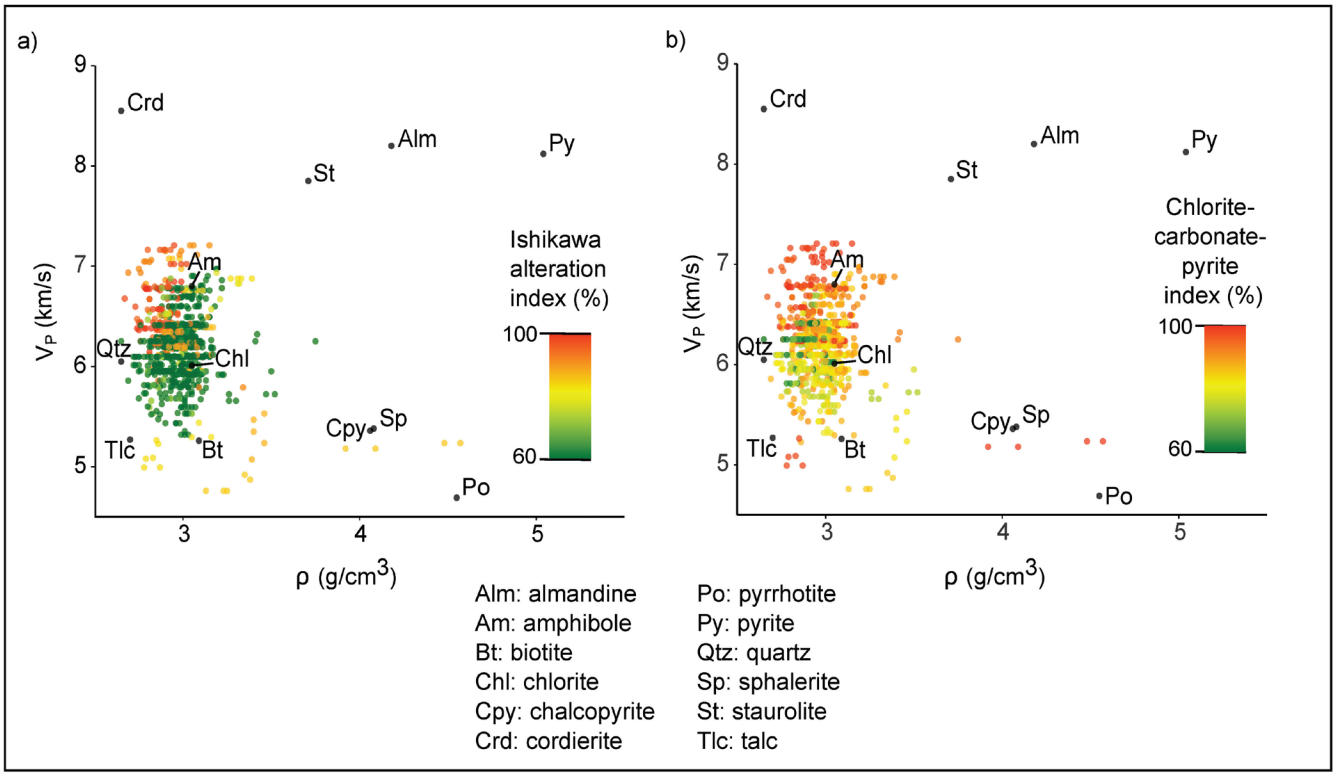

Figure 3. P-wave velocity (V_p) and density (ρ) of rocks with intermediate to mafic volcanic protoliths from the footwall of the Lalor volcanogenic massive-sulfide deposit. Points are coloured according to **a)** the Ishikawa alteration index (AI) and **b)** the chlorite-carbonate-pyrite index (CCPI).

these assumptions, the effects of mineral composition on seismic rock properties can be modelled by combining the bulk mineral fractions (f_i) with their corresponding mineral P-wave velocities (V_{p_i}) and densities (ρ_i; Table 3) to obtain mixture-modelled bulk seismic rock properties (Schetselaar et al., 2019).

A comparison between the mixture-modelled seismic rock properties and laboratory measurements of seismic properties of drill core (Table 4) shows, with the exception of two outliers, a good fit for density (Fig. 5a) and a reasonable fit for P-wave velocity, which was modelled using the average of the Voigt and Reuss bounds (Fig. 5b; Schetselaar et al., 2019). A V_p-ρ plot of measured rock and mineral seismic properties shows that the most abundant minerals positioned beyond the extremes of the measured V_p-ρ distribution, along the approximately perpendicular biotite-cordierite and quartz-garnet bivariate mixture lines, dominantly control the seismic rock property variations (Fig. 6). Although the SEM-EDS sample set is limited, the relatively large average abundance of low-density, high-velocity cordierite (Fig. 7a) and its positive correlation with P-wave velocity (Fig. 7b) is consistent with the low-density trends of intensely altered intermediate to mafic lithofacies (Fig. 2), as well as increasing alteration index values toward higher velocities (Fig. 3). Cordierite and other aluminosilicates, such as garnet, kyanite, sillimanite, and staurolite in volcanic protoliths, are diagnostic of hydrothermally altered rocks that have been metamorphosed in the middle to upper amphibolite facies (Menard and Gordon, 1997; Caté, 2016). Cordierite has a unique low-density, high P-wave velocity signature in comparison to other silicate minerals, which explains the negative low-density, high P-wave velocity trend (Fig. 2, 3, and 6). In general, the SEM-EDS results confirm that seismic rock property variations in the host rocks of the Lalor VMS deposit are controlled by large variations in the abundance of silicates, with sulfides having negligible effects (Table 2).

TWO-DIMENSIONAL SEISMIC SYNTHETICS

The impact of high-velocity aluminosilicates on reflectivity was further assessed by modelling the seismic response of a simple VMS deposit within a bimodal volcanic host rock package (e.g. basalt and rhyolite), a volcanogenic massive-sulfide ore lens, and a subconcordant hydrothermal conduit (Fig. 8). Two scenarios were tested: a model in which the grade of the metamorphic overprint corresponds to peak metamorphic conditions recorded for the Lalor deposit (600ºC, 6 kbar; Caté, 2017) and a low-grade greenschist-facies (350ºC, 2.5 kbar) equivalent of the

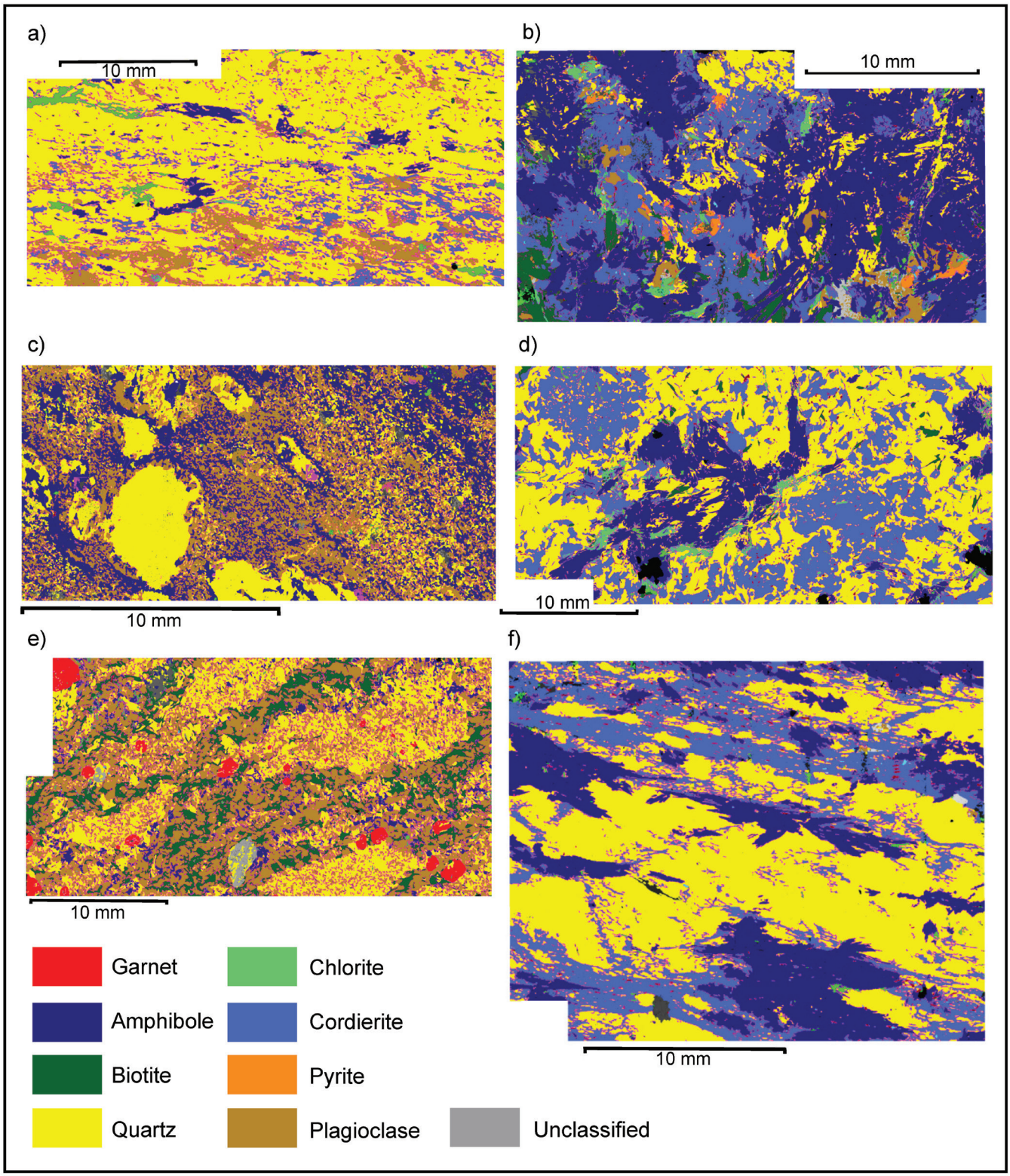

Figure 4. Scanning electron microscopy–energy dispersive X-ray spectrometry mineral maps of six thin sections: **a)** GSC-Lalor-MD038, **b)** GSC-Lalor-MD041, **c)** GSC-Lalor-MD156, **d)** GSC-Lalor-MD165, **e)** GSC-Lalor-MD188, and **f)** GSC-Lalor-MD218.

Contents

Table 2. Scanning electron microscopy–energy dispersive X-ray spectrometry analyses of thin sections from drill-core samples from the Lalor volcanogenic massive-sulfide deposit subjected to laboratory measurements of seismic rock properties.

Sample	Lithology	Am	An	Ap	Bt	Cal	Dol	Ccp	Chl	Crd	Ep	Gr	Grt	Hbl	Ilm	Py	Qtz	Rt	Sil	St	Undef	Total
GSC-Lalor-MD-023	Anthophyllite-cordierite-garnet gneiss	8.9	7.2	0.2	10.7	0.1	0	0.1	1.1	36.3	0	0.1	7.6	0	0.4	1	24.3	0	0	0	2.3	100.3
GSC-Lalor-MD-038	Rhyolite	2.9	10.1	0	0	0	0	0	12.6	1.8	0	0	0	0	0.1	0	68.2	0	0	0	4.3	100
GSC-Lalor-MD-039	Rhyolite	0	1.6	0	7.7	0	0	0	0.1	0	0	0.1	0	0	0	0.6	81.6	0	1.3	2.2	5	100.1
GSC-Lalor-MD-041	Biotite-staurolith-garnet schist	53.2	0	0.2	4.8	0	0	0	2	21.7	0	0	0	0	0.4	3.1	11.7	0	0	1	1.9	100
GSC-Lalor-MD-099	Anthophyllite-cordierite-garnet gneiss	17.9	8.9	0.5	2	0	0	0	1.8	19.9	0	0	13.7	0.1	0.8	2.4	29.9	0	0	0.2	1.9	100
GSC-Lalor-MD-110	Anthophyllite-cordierite gneiss	46.7	0	0.3	6.3	0	0	0	11.2	27.4	0	0	0	0.1	0.8	1.4	3.7	0.5	0	0.5	1.1	100.1
GSC-Lalor-MD-156	Basalt	0	34.8	0	3	0	0	0.2	0	0	0	0	0	36.6	0.2	0	27.7	0	0	0	0.5	103
GSC-Lalor-MD-160	Quartz-biotite-cordierite gneiss	7.5	0	0.4	29.6	0	0	0	1.8	20.4	0	0	0	0	1.7	0	37.4	0	0	0	1	100
GSC-Lalor-MD-165	Biotite-garnet-anthophyllite gneiss	14.9	0	0.2	1.3	0	0	0	2.7	32.7	0	0	0	0	0.6	0	45.8	0	0	0	1.8	100
GSC-Lalor-MD-188	Felsic tuff	5.5	38.7	0.1	18.8	0	0	0	0	0	0	0	2.6	0	0.1	0	32.9	0	0	0	1.4	100
GSC-Lalor-MD-218	Anthophyllite-cordierite gneiss	24.1	0	0.2	0	0	0	0	0	26.2	0	0	0	0	0.6	0.1	48.3	0	0	0	0.6	100
Mean		16.5	9.2	0.2	7.7	0	0	0	3	16.9	0	0	2.2	3.4	0.5	0.8	37.4	0	0.1	0.4	2	100.3
Mineral abundances are given in volume per cent.																						

Table 3. Seismic properties of selected minerals.

Mineral	Abbreviation	Density (g/cm³)	P-wave velocity (km/s)	P-wave velocity anisotropy (%)	Shear wave velocity (km/s)	Bulk modulus (GPa)	Shear modulus (GPa)
Albite	Ab	2.63[1]	6.30[2]	30.9[2]	3.70[2]	68.38	86.25
Anorthite	An	2.73[3]	7.25[2]	31.8[2]	4.30[2]	93.02	134.05
Amphibole	Am	2.95[3]	6.95[2]	23.8[2]	3.85[2]	98.77	103.02
Biotite	Bt	3.09[3]	5.26[2]	–	2.87[3]	60.04	43.33
Chlorite	Chl	3.05[3]	6.01[4]	–	3.00[4]	82.72	54.09
Cordierite	Crd	2.65[4]	8.71[5]	14.2[5]	4.51[5]	147.14	177.16
Epidote	Ep	3.40[1]	7.43[1]	19.9[2]	4.25[2]	126.28	134.2
Garnet	Grt	4.20[3]	8.55[2]	0.9[2]	4.75[2]	212.27	192.91
Pyrite	Py	5.04[6]	8.12[6]	–	4.95[6]	208.82	198.96
Quartz	Qtz	2.65[4]	6.05[3]	23.6[2]	4.09[2]	52.67	101.21
Sericite	Ser	2.81[4]	6.30[2]	44.2[2]	3.75[2]	72.01	88.59
Sillimanite	Sil	3.24[3]	9.70[2]	22.7[2]	5.35[2]	212.11	277.64
Staurolite	St	3.71[3]	7.85[2]	34.5[2]	4.65[2]	148.4	169.74

[1]Mavko et al., 2009 [2]Ji et al., 2002 [3]Barthelmy, 2014 [4]Kern et al., 2009 [5]Toohill et al., 1999 [6]Salisbury et al., 2000

first model, representative of most of the VMS deposits in the Canadian Shield. Seismic properties of the first model were computed from the mineral fractions of seven samples from the zone of intense hydrothermal alteration (Schetselaar et al., 2019; Table 3). Normative minerals computed from major oxide analyses of the same samples using CONSONORM_LG (Trépanier et al., 2015) were used to compute seismic properties of the conduit at the lower greenschist-facies for the second scenario. The normative minerals obtained for the conduit of the greenschist-facies synthetic model were generalized into fewer classes and renormalized to 1. This involved omission of all the fractions below 1 volume %, summation of magnesium chlorite and iron chlorite, and summation of paragonite and sericite. Properties of least-altered host rocks and ore for the greenschist-facies modelling scenario were determined from wireline logs of least-altered basalt and rhyolite from acquired in the Flin Flon VMS camp (White et al., 2016). The seismic properties of the modelled units are listed in Table 5.

A total of 40 shot points equally distributed 20 m below the surface were modelled with an acoustic (P-wave velocity and density) finite-difference method based on a second-order approximation of the time derivatives and a fourth-order approximation of the spatial derivatives solved on a staggered grid. The seismic wavefield was sampled at 341 receivers placed every 10 m near the surface of the model. The seismic source is a Ricker wavelet with a centre frequency of 70 Hz, which corresponds to the centre frequency of the Lalor migrated volume (Bellefleur et al., 2015). Synthetic shot gathers were then migrated in depth using a reverse time algorithm. Modelling and reverse time migration were conducted using Devito (Louboutin et al., 2019). The strongest reflections are in both the greenschist- and amphibolite-facies scenarios, associated with the ore zone (Fig. 8, Table 6).

For the amphibolite scenario, the reflection beneath the ore zone includes constructive interference from the conduit-basalt contact. Note the enhanced reflectivity of the basalt-rhyolite contacts in the amphibolite-facies scenario due to a significant increase in the P-wave velocity of basalt (a 40% increase in reflectivity compared to the greenschist scenario; Table 5). The most significant difference in acoustic impedance contrast between the two scenarios is observed at contacts between the conduit and felsic host rocks. The reflectivity of the conduit-rhyolite contacts increases by 75% (Table 6) for the amphibolite scenario compared to the greenschist scenario, becoming as great as the impedance contrast across basalt-rhyolite contacts (Table 5). In contrast, in the greenschist scenario, the conduit is weakly reflective when juxtaposed against rhyolite. Seismic reflections at conduit-basalt contacts are probably not detectable in both scenarios, considering the 6% rule-of-thumb threshold for a strong seismic reflection (Snyder and Salisbury, 2007).

Table 4. Zr-Ti ratio, alteration indices, and measured and modelled seismic rock properties of samples from the Lalor volcanogenic massive-sulfide deposit.

Sample	Lithology	Zr-Ti ratio	Ishikawa alteration index	Chlorite-carbonate-pyrite index	Measured density (g/cm^3)	Measured P-wave velocity (km/s)	Modelled density (g/cm^3)	Modelled P-wave velocity (km/s)
GSC-Lalor-MD-023	Anthophyllite-cordierite-garnet gneiss	0.012	69.66	85.05	2.85	7.32	2.86	7.12
GSC-Lalor-MD-038	Rhyolite	0.058	88.74	97.76	2.72	6.33	2.72	6.16
GSC-Lalor-MD-039	Rhyolite	–	–	–	2.71	6.81	2.72	6.06
GSC-Lalor-MD-041	Biotite-staurolite-garnet schist	0.017	90.96	91.49	2.94	6.86	2.98	7.06
GSC-Lalor-MD-099	Anthophyllite-cordierite-garnet gneiss	0.012	65.43	95.83	3.00	6.94	2.96	7.07
GSC-Lalor-MD-110	Anthophyllite-cordierite gneiss	0.014	95.61	96.66	2.86	7.57	2.87	7.08
GSC-Lalor-MD-156	Basalt	0.013	31.83	82.76	3.00	6.71	2.92	6.72
GSC-Lalor-MD-160	Quartz-biotite-cordierite gneiss	0.027	95.05	92.44	2.77	6.77	2.82	6.26
GSC-Lalor-MD-165	Biotite-garnet-anthophyllite gneiss	0.031	90.72	88.12	2.88	6.24	2.71	6.88
GSC-Lalor-MD-188	Felsic tuff	0.027	52.67	74.81	2.86	6.18	2.82	6.38
GSC-Lalor-MD-218	Anthophyllite-cordierite gneiss	0.009	88.45	99.58	2.86	7.20	2.72	6.82
Mean		0.020	76.91	90.45	2.86	6.81	2.83	6.69

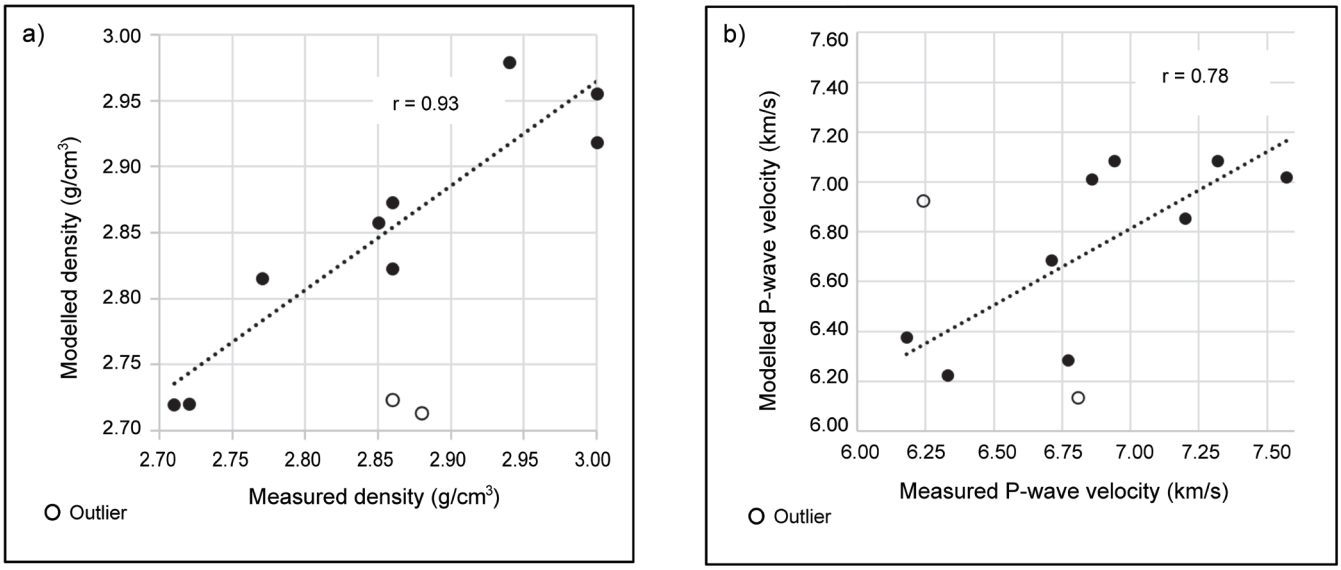

Figure 5. Scatterplots comparing modelled seismic rock properties to those measured from drill core; outliers were not considered during regression analysis: **a)** density (ρ); **b)** P-wave velocity (V_p), modelled using the average of Voigt and Reuss bounds (*see* Schetselaar et al. (2019) for the definition and computation of Voigt and Reuss bounds).

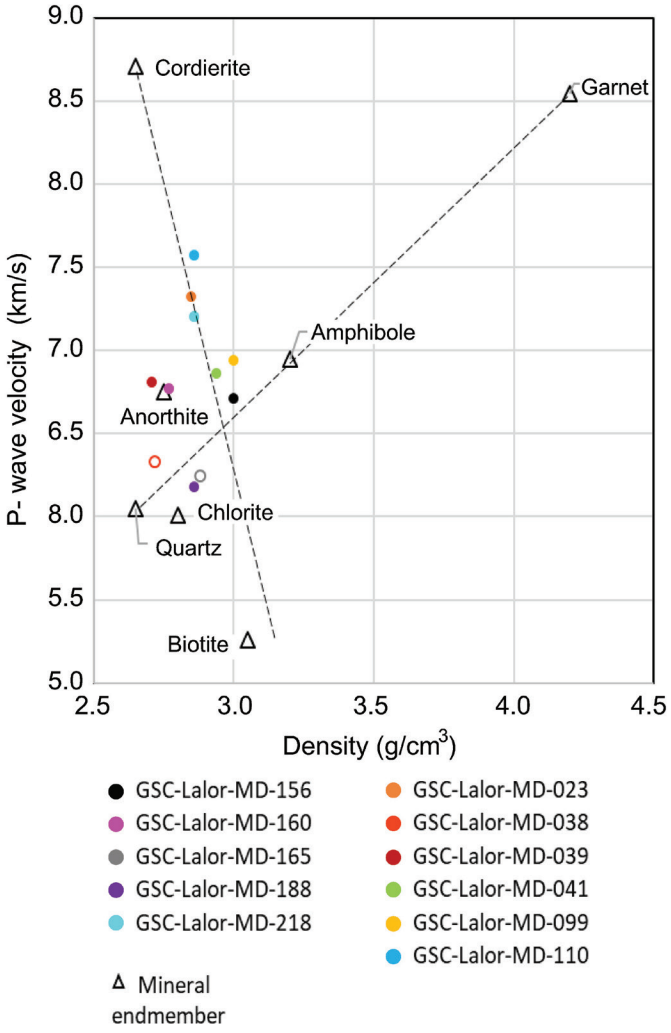

Figure 6. P-wave velocity (V_p)–density (ρ) plot of seismic rock properties from mixture modelling and endmembers from the literature corresponding to minerals listed in Table 3.

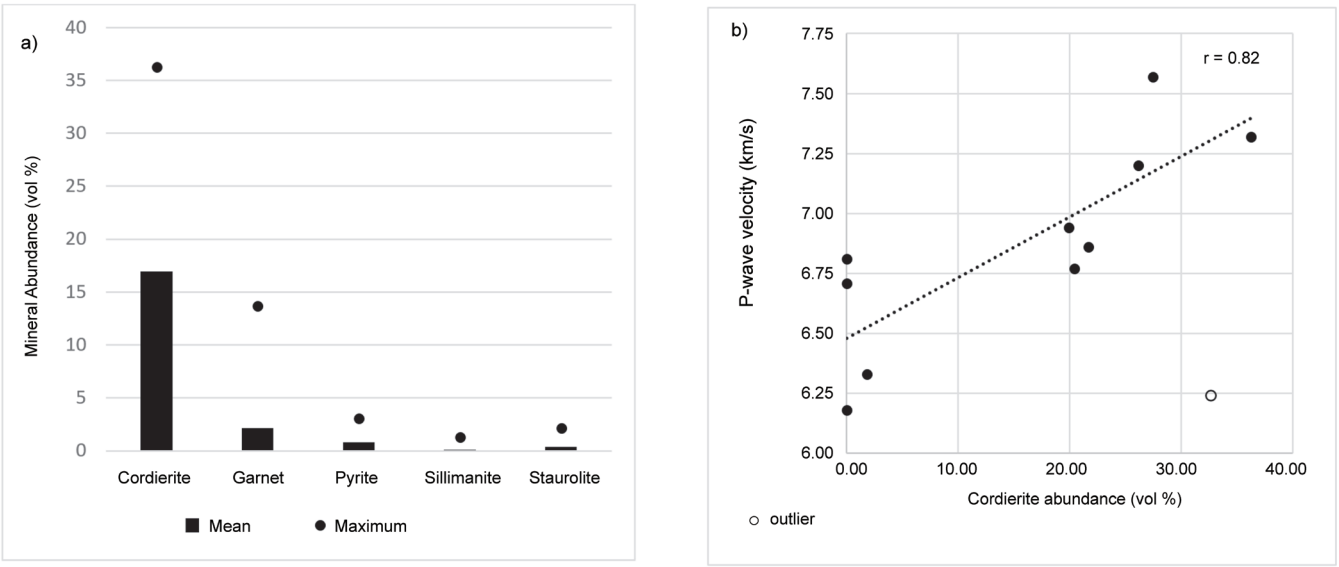

Figure 7. Summary of scanning electron microscopy–energy dispersive X-ray spectrometry analyses of high–P-wave velocity (V_p) minerals (V_p > 7.5 km/s) from samples of the hydrothermal alteration zone: **a)** volume percentages of high-V_p minerals; **b)** the relationship between cordierite abundance and P-wave velocity (V_p).

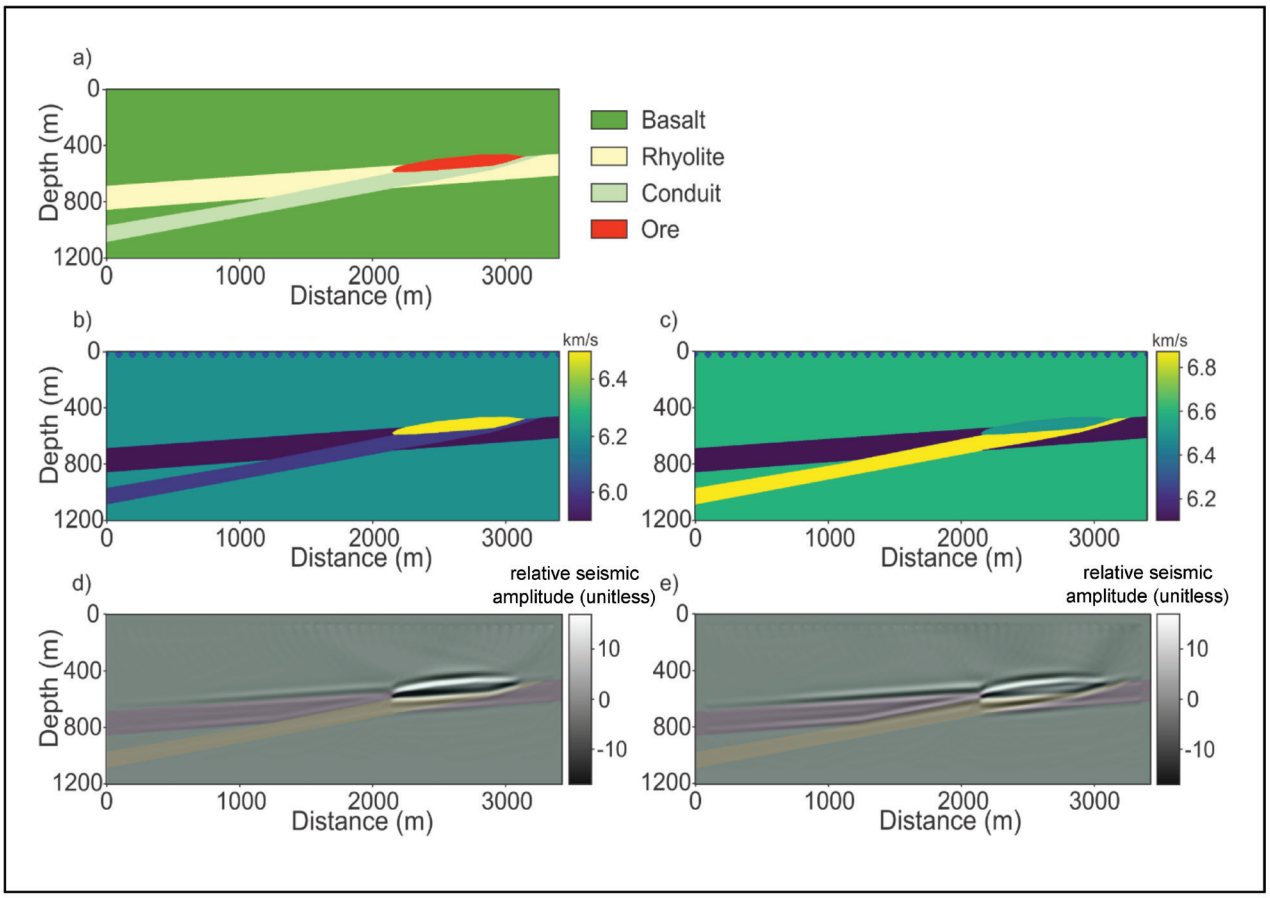

Figure 8. Models used for seismic synthetics: **a)** model of a volcanogenic massive-sulfide deposit with subconcordant hydrothermal conduit; **b)** P-wave velocity model for greenschist-facies conditions; **c)** P-wave velocity model for amphibolite-facies conditions; **d)** processed seismic forward modelling profile for greenschist-facies conditions; and **e)** processed seismic forward modelling profile for amphibolite conditions. *See* text for details of the modelling procedure.

Table 5. Seismic rock properties used for synthetic modelling.

Amphibolite facies						Greenschist facies				
Unit	**Mineral**	**Abundance (vol %)**	**Density (g/cm³)**	**P-wave velocity (km/s)**	**Acoustic impedance (kg·m⁻²s⁻¹ × 0⁻⁶)**	**Mineral**	**Abundance (vol %)**	**Density (g/cm³)**	**P-wave velocity (km/s)**	**Acoustic impedance (kg·m⁻²s⁻¹ × 0⁻⁶)**
Conduit	Cordierite	28	2.65	8.71	23.1					
	Garnet	3	4.2	8.55	35.9	Epidote	4	3.4	7.43	25.3
	Amphibole	27	2.95	6.95	20.5	Chlorite	47	3.05	6.01	18.3
	Biotite	9	3.15	5.26	16.6	Sericite	10	2.81	6.3	17.7
	Anorthite	3	2.73	7.25	19.8	Albite	2	2.63	6.3	16.6
	Quartz	30	2.65	6.05	16	Quartz	37	2.65	6.05	16
	Pyrite	1	5.04	8.12	40.9	Pyrite	1	5.04	8.12	40.9
	Mixture modelled		2.88	6.87	19.8	Mixture modelled		2.9	6.01	17.4
Basalt			3	6.6	19.8			2.9	6.2	18
Rhyolite			2.8	6.1	17.1			2.75	5.9	16.2
Ore			4.2	6.5	27.3			4.2	6.5	27.3

Table 6. Coefficients of seismic reflectivity (R) for contacts between ore, conduit, and host rocks (Fig. 8a) for the greenschist- and amphibolite-facies acoustic finite difference models.

Model contact (Fig. 8a)	Greenschist facies R (%)	Amphibolite facies R (%)	Difference (%)
Sulfide ore-basalt	21	16	–24
Sulfide ore-rhyolite	26	23	–12
Basalt-rhyolite	5	7	40
Conduit-basalt	2	0	–∞
Conduit-rhyolite	4	7	75

SEISMIC INTERPRETATION

In 2013, the Geological Survey of Canada carried out a 3-D seismic survey to characterize the 3-D structure of the Lalor deposit and its host rock envelope (Bellefleur et al. (2015). The survey covered an area of approximately 16 km^2 (Fig. 1) and included 908 shot points and 2685 receiver stations. Many shot points northeast of the deposit provided sufficient ore zone illumination from the downdip direction to produce a high-quality image of the deposit and hydrothermal alteration zone. Details of the acquisition, data processing, and initial interpretation of the 3-D seismic data are reported in Bellefleur et al. (2015). The seismic survey detected the massive Zn-rich zones and identified strong reflectivity in altered footwall rocks at contacts between metamorphosed rocks with felsic and mafic protoliths (Bellefleur et al., 2015). Figure 9 shows a cross section of inline 1098 from the 3-D seismic volume and a coincident section from a 3-D geological model representing lithofacies derived from ratios of immobile elements. Arrows A and B point to reflections occurring at contacts between felsic and mafic rocks/protoliths in the least-altered and intensely altered footwall rocks. Reflection B has higher amplitudes and is more continuous than reflection A. Arrow C indicates a series of strong reflections downdip of the alteration zone in the geological model and represents a possible continuation of strong footwall alteration at depth. Following our interpretation, areas indicated by arrow C and possibly arrow D are rocks characterized by intense hydrothermal alteration and have high exploration potential. At Lalor, examples of such potential are the disseminated gold-rich zones that, contrary to the massive-sulfide zones of this deposit, are not directly detectable by seismic or other geophysical methods. This is because these relatively narrow zones with low sulfide content do not sufficiently change seismic rock properties to generate reflections. The disseminated zones nevertheless occur in metamorphosed and altered footwall rocks characterized by enhanced seismic reflectivity originating from hydrothermally altered rocks with significant abundance of aluminosilicate minerals with high V_p (cordierite and garnet).

DISCUSSION

Four distinct processes controlled the seismic rock properties throughout the geological history of the Lalor VMS deposit: 1) protolith composition of the volcanic and volcaniclastic rocks, 2) host rock hydrothermal alteration during subsequent circulation of seafloor hydrothermal fluids through the host rocks, 3) sulfide mineralization at or

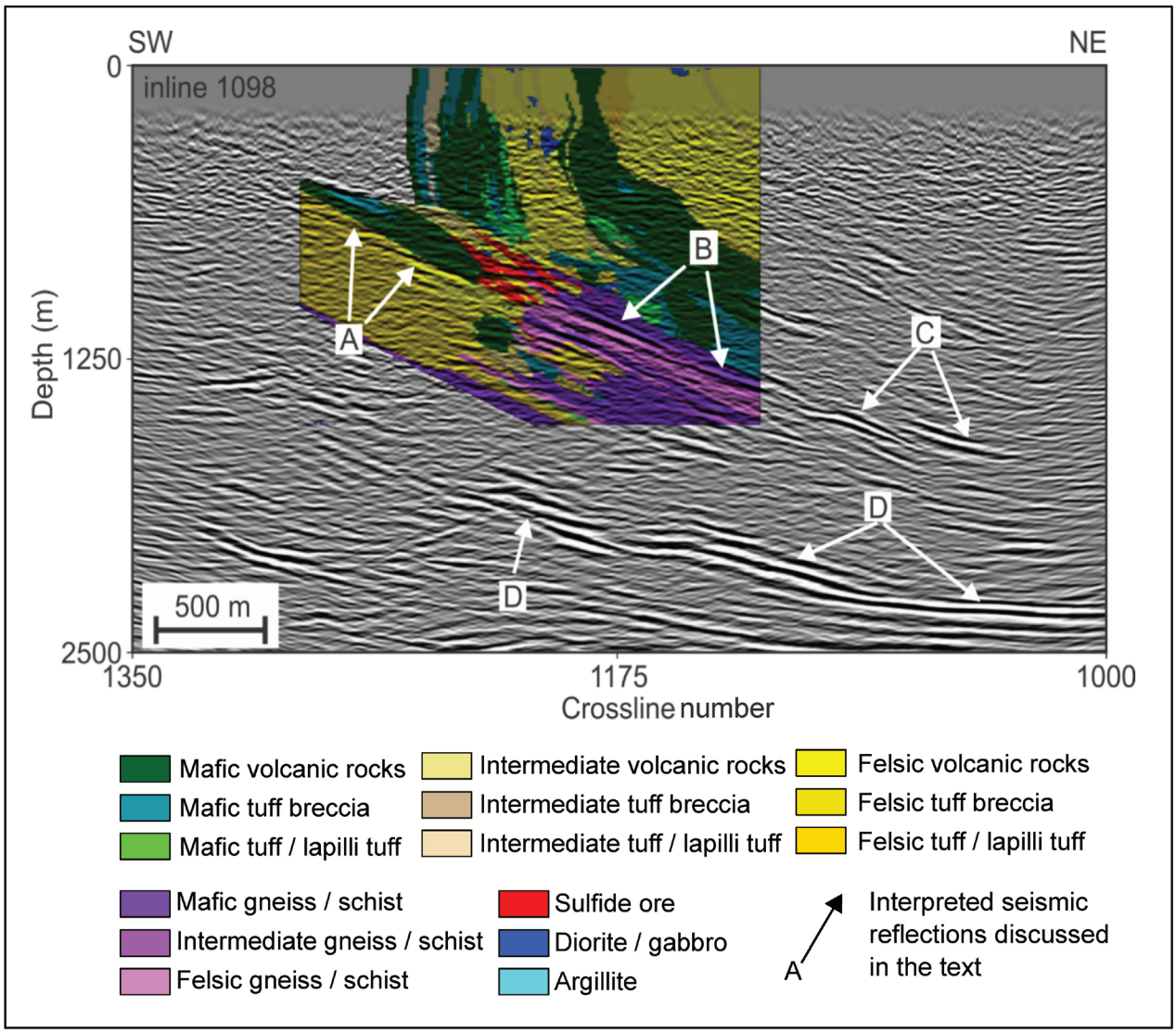

Figure 9. Inline 1098 from the final migrated seismic volume overlain with a coincident section from the 3-D geological model in colour. *See* text for details of events indicated by arrows. *Modified from* Schetselaar et al. (2017).

near the ocean floor, and 4) metamorphic recrystallization of host rocks and ore after emplacement and subsequent tectonic burial of the VMS deposit within an orogenic belt.

All four processes (in addition to weathering and unloading when the deposit was exhumed) affected seismic rock properties, although the first two appear to have been dominant; hence, they are dominantly reported in the hard-rock seismic exploration literature (Salisbury et al., 2000; Snyder and Salisbury, 2007; Malehmir et al., 2012). The additional effects of the latter two processes on seismic rock properties are much more challenging to assess. Compared to the few sulfide species that define the ore zones, far more silicate species, many of which are also found in their unaltered equivalents, occur in association with VMS deposits. Many of the silicates involved have much stronger anisotropies in velocity and will likely react to other species as a result of subsequent metamorphic recrystallization. The SEM-EDS analysis, although applied on a limited number of samples (n = 11), was effective for interpreting the relationships between mineral abundance and laboratory measurements of seismic rock properties of hydrothermally altered rocks and allowed corroboration of the empirical relationships inferred from the much larger wireline seismic property data sets.

Expected benefits of the analysis of the relationships between seismic rock property measurements and geochemical proxies for alteration, as previously attempted in Schetselaar et al. (2018), are limited in scope because, as shown in the seismic forward modelling study, similar ranges in these proxies could show large variations in mineral seismic properties, depending on metamorphic grade. Estimates of mineral abundance are, therefore, essential to improving understanding of the seismic response of hydrothermal

alteration. A solution that would bypass laborious mineralogical analysis is to obtain theoretical mineral-abundance estimates though normative mineral computation, but these methods are fraught with modelling limitations themselves because they either lead to non-unique solutions or, when additional constraints (e.g. pressure, temperature) are considered, they yield mineral species that significantly deviate from those actually present. Future studies may explore upscaling approaches, where the results of the SEM-EDS analyses are used to define the endmembers in user-defined normative mineral computations, such as those proposed in Currie (1991).

CONCLUSIONS

The effects of hydrothermal alteration and subsequent metamorphic recrystallization on density, P-wave velocity, and seismic response of the Lalor VMS deposit have been investigated using lithofacies log descriptions, density, and P-wave velocity logs in combination with alteration indices from whole rock geochemistry and SEM-EDS mineral abundance estimates. These analyses show that the metamorphosed footwall alteration zone of the Lalor VMS deposit is marked by a steep, low-density trend toward V_p = 8.71 km/s and ρ = 2.65 g/cm^3, corresponding to the seismic properties of cordierite, which has a unique low-density, high P-wave velocity signature atypical of any other silicate mineral. The SEM-EDS analysis of thin sections show that cordierite, with its anomalous high bulk modulus over density ratio, is the most abundant high-velocity mineral, which further corroborates the interpretation that the steep V_p-ρ alteration signature is due to cordierite. Metamorphosed hydrothermal alteration zones with high abundances of cordierite and other high P-wave velocity aluminosilicate minerals such as garnet, kyanite, sillimanite, and staurolite may, therefore, be detectable seismic targets.

ACKNOWLEDGMENTS

We gratefully acknowledge the support of HudBay Minerals Inc. in providing access to the drillhole data from the Lalor mine camp and for sharing their expertise on the Lalor VMS deposit. We are grateful to Antoine Caté and Patrick Mercier-Langevin for sharing their expertise on the geology of the Lalor VMS deposit and their assistance in preparing drill-core sample materials for whole-rock geochemical and SEM-EDS analysis. We thank Randy Enkin and Matt Salisbury for conducting laboratory drill-core physical rock property measurements. This paper benefitted from discussions with Don White and Rob Berman, as well as the critical comments of reviewers Don White and Bernd Milkereit. We acknowledge funding of this research by Natural Resources Canada's Targeted Geoscience Initiative program (phase 4 and phase 5). Editorial handling was done by Jan Peter.

REFERENCES

Bailes, A.H. and Galley, A.G., 1999. Evolution of the Paleoproterozoic Snow Lake arc assemblage and geodynamic setting for associated volcanic-hosted massive sulphide deposits, Flin Flon Belt, Manitoba, Canada; Canadian Journal of Earth Sciences, v. 36, no. 11, p. 1789−1805. https://doi.org/10.1139/e98-111

Bailes, A.H., Galley, A.G., Paradis, S., and Taylor, B.E., 2016. Variations in large synvolcanic alteration zones at Snow Lake, Manitoba, Canada, with proximity to associated volcanogenic massive sulfide deposits; Economic Geology, v. 111, no. 4, p. 933–962. https://doi.org/10.2113/econgeo.111.4.933

Barthelmy, D.; 2014, Mineral properties, <http://webmineral.com/determin.shtml> [accessed March 12, 2019]

Bellefleur, G., Schetselaar, E., White, D., Miah, K., and Dueck, P., 2015. 3D seismic imaging of the Lalor volcanogenic massive sulphide deposit, Manitoba, Canada; Geophysical Prospecting, v. 63, no. 4, p. 813–832. https://doi.org/10.1111/1365-2478.12236

Caté, A., 2016. Geology of the Paleoproterozoic Zn-Cu-Au Lalor volcanogenic massive sulphide deposit and its gold-rich lenses, Snow Lake, Manitoba; PhD thesis, Université du Québec, Institut National de la Recherche Scientifique, Québec, Canada, 430 p.

Caté, A., Mercier-Langevin, P., Ross, P.S., Duff, S., Hannington, M., Dubé, B., and Gagné, S., 2014. The Paleoproterozoic Lalor VMS deposit, Snow Lake, Manitoba: observations on the nature and architecture of the gold and base metal-rich ore zones and associated alteration; Geological Survey of Canada, Open File Report 7483, 19 p. https://doi.org/10.4095/293116

Currie, K.L., 1991. GENORM: a generalized norm calculation; Computers & Geosciences, v. 17, no. 1, p. 77–89. https://doi.org/10.1016/0098-3004(91)90080-W

Ji, S., Wang, Q., and Xia, B., 2002. Handbook of seismic properties of minerals, rocks and ores; Polytechnic International Press, Montreal, 630 p.

Kern, H., Mengel, K., Strauss, K.W., Ivankina, T.I., Nikitin, A.N., and Kukkonen, I.T., 2009. Elastic wave velocities, chemistry and modal mineralogy of crustal rocks sampled by the Outokumpu scientific drill hole: evidence from lab measurements and modelling; Physics of the Earth and Planetary Interiors, v. 175, no. 3–4, p. 151–166. https://doi.org/10.1016/j.pepi.2009.03.009

Kraus, J. and Williams, P.F., 1999. Structural development of the Snow Lake allochthon and its role in the evolution of the southeastern Trans-Hudson Orogen in Manitoba, central Canada; Canadian Journal of Earth Sciences, v. 36, no. 11, p. 1881–1899. https://doi.org/10.1139/e99-014

Large, R.R., Gemmell, J.B., Paulick, H., and Huston, D.L., 2001. The alteration box plot: a simple approach to understand the relationship between alteration mineralogy and lithogeochemistry associated with volcanic-hosted massive sulfide deposits; Economic Geology, v. 96, no. 5, p. 957–971. https://doi.org/10.2113/gsecongeo.96.5.957

Louboutin, M., Lange, M., Luporini, F., Kukreja, N., Witte, P.A., Herrmann, F.J., Velesko, P., and Gorman, G.J., 2019. Devito (v3.1.0): an embedded domain-specific language for finite differences and geophysical exploration; Geoscience Model Development, v. 12, no. 3, p. 1165–1187. https://doi.org/10.5194/gmd-12-1165-2019

Malehmir, A., Durrheim, R., Bellefleur, G., Urosevic, M., Juhlin, C., White, D.J., Milkereit, B., and Campbell, G., 2012. Seismic methods in mineral exploration and mine planning: a general overview of past and present case histories and a look into the future; Geophysics, v. 77, no. 5, p. WC173–WC190. https://doi.org/10.1190/geo2012-0028.1

Mavko, G., Mukerji, T., and Dvorkin, J., 2009. The rock physics handbook, 2nd edition: tools for seismic analysis of porous media; Cambridge University Press, Cambridge, UK, 511 p.

Menard, T. and Gordon, T.M., 1997. Metamorphic P-T paths from the eastern Flin Flon belt and Kisseynew domain Snow Lake, Manitoba; The Canadian Mineralogist, v. 35, no. 5, p. 1093–1115.

Oxford Instruments, Automated analysis of sections of geological materials; Oxford Instruments. <https://nano.oxinst.com/campaigns/downloads/automated-analysis-of-sections-of-geological-materials> [accessed May 15, 2019]

Oxford Instruments, 2020. EDS for SEM and FIB; Oxford Instruments. <https://nano.oxinst.com/campaigns/downloads/automated-analysis-of-sections-of-geological-materials> [accessed April 14, 2020]

Salisbury, M.H., Milkereit, B., and Bleeker, W., 1996. Seismic imaging of massive sulfide deposits; Part I, Rock properties; Economic Geology, v. 91, no. 5, p. 821–828.

Salisbury, M.H., Milkereit, B., Ascough, G., Adair, R., Matthews, L., Schmitt, D.R., Mwenifumbo, J., Eaton, D.W., and Wu, J., 2000. Physical properties and seismic imaging of massive sulphides; Geophysics, v. 65, no. 6, p. 1882–1889. https://doi.org/10.1190/1.1444872

Schetselaar, E., Bellefleur, G., Craven, J., Roots, E., Cheraghi, S., Shamsipour, P., Caté, A., Mercier-Langevin, P., El Goumi, N., Enkin, R., and Salisbury, M., 2017. Geologically driven 3D modelling of physical rock properties in support of interpreting the seismic response of the Lalor volcanogenic massive sulphide deposit, Snow Lake, Manitoba, Canada; *in* Characterization of ore-forming systems from geological, geochemical and geophysical studies, (ed.) K. Gessner, T.G. Blenkinsop, and P. Sorjonen-Ward; Geological Society of London, Special Publication 453, p. 57–82. https://doi.org/10.1144/SP453.5

Schetselaar, E.M., Bellefleur, G., Craven, J.A., Ansari, S.M., and Enkin, R.J., 2018. Elucidating mineralizing fluid pathways from the geophysical responses to hydrothermal alteration: integrated 3D modelling of lithogeochemical, petrophysical, seismic and magnetotelluric data, Lalor volcanogenic massive sulphide deposit, Manitoba; *in* Targeted Geoscience Initiative: 2017 report of activities, volume 1, (ed.) N. Rogers; Geological Survey of Canada, Open File 8358, p. 229–242. https://doi.org/10.4095/306479

Schetselaar, E.M., Bellefleur, G., and Hunt, P., 2019. Elucidating the effects of hydrothermal alteration on seismic reflectivity in the footwall of the Lalor volcanogenic massive sulfide deposit, Snow Lake, Manitoba, Canada; Minerals, v. 9, no. 6, 384, 23 p. https://doi.org/10.3390/min9060384

Snyder, D. and Salisbury, M.H., 2007. Application of seismic methods to mineral exploration; *in* Mineral deposits of Canada: a synthesis of major deposit-types, district metallogeny, the evolution of geological provinces, and exploration methods, (ed.) W.D. Goodfellow; Geological Association of Canada, Mineral Deposits Division, Special Publication No. 5, p. 971–982.

Stewart, M.S., Lafrance, B., and Gibson, H.L., 2018. Early thrusting and folding in the Snow Lake camp, Manitoba: tectonic implications and effects on volcanogenic massive sulfide deposits; Canadian Journal of Earth Sciences, v. 55, no. 8, p. 935–957. https://doi.org/10.1139/cjes-2017-0242

Toohill, K., Siegesmund, S., and Bass, J.D., 1999. Sound velocities and elasticity of cordierite and implications for deep crustal seismic anisotropy; Physics and Chemistry of Minerals, v. 26, p. 333–343. https://doi.org/10.1007/s002690050193

Trépanier, S., Mathieu, L., and Daigneault, R., 2015. CONSONORM_LG: new normative minerals and alteration indices for low-grade metamorphic rocks; Economic Geology, v. 110, no. 8, p. 2127–2138. https://doi.org/10.2113/econgeo.110.8.2127

White, D.J., Mwenifumbo, C.J., and Salisbury, M.H., 2016. Seismic properties of rocks from the Flin Flon volcanogenic massive sulfide camp; Economic Geology, v. 111, no. 4, p. 913–931. https://doi.org/10.2113/econgeo.111.4.913